ResearchGate

See discussions, stats, and author profiles for this publication at: https://www.researchgate.net/publication/231643901

Site-Specific Deposition of Titanium Oxide on Zinc Oxide Nanorods

ARTICLE *in* THE JOURNAL OF PHYSICAL CHEMISTRY C · OCTOBER 2007

Impact Factor: 4.77 · DOI: 10.1021/jp0756911

CITATIONS
18

READS
34

5 AUTHORS, INCLUDING:

Cheng C
South University of Science and Technology …
55 PUBLICATIONS **723** CITATIONS
SEE PROFILE

Ning Wang
Fujian Medical University
176 PUBLICATIONS **3,386** CITATIONS
SEE PROFILE

Available from: Cheng C
Retrieved on: 03 February 2016

Site-Specific Deposition of Titanium Oxide on Zinc Oxide Nanorods

Chun Cheng, Kai Feng Yu, Yuan Cai, Kwok Kwong Fung, and Ning Wang*

Department of Physics and the Institute of Nano Science and Technology, the Hong Kong University of Science and Technology, Hong Kong, China

Received: July 20, 2007; In Final Form: August 28, 2007

ZnO/TiO_2 nanohybrid structures have been synthesized by the simple method of the site-specific deposition of titanium oxide on ZnO nanorods. The polarity of the ZnO (0001) surface plays an important role in the formation of the nanohybrid structures. Using high-resolution transmission electron microscopy, we observed that the amorphous TiO_2 particles that are connected to ZnO nanorods are transformed to nanocrystals of the anatase and rutile phases, which have a particular relationship with the orientation of ZnO nanorods and good interface structures. This work provides a rational approach to the assembly of complex nanohybrids using the intrinsic properties of ZnO nanocrystals. In addition, the size, aspect ratio, and TiO_2 structures can be fully controlled in the fabrication process and subsequent annealing treatments.

Introduction

Semiconductor nanostructured composites are of interest in many technological applications, such as biolabels, electroluminescent displays, photochemical solar cells, photocatalysis, and sensors. In recent years, considerable effort has been devoted to combining semiconductor nanoparticles with suitable materials to synergize the properties of both components, which has led to many promising applications such as the enhancement of photocatalytic performance through the deposition of metal or metal islands on ZnO and TiO_2 nanoparticles.[1,2] In general, photocatalytic efficiency is limited by the fast recombination of photogenerated charge carriers. In semiconductor/metal nanocomposites, the photoinduced charge carriers are trapped by the metal component, which promotes interfacial charge-transfer processes.[3] Compared to pure ZnO and TiO_2, coupled ZnO/TiO_2 polycrystals display a greater photocatalytic activity, such as in the degradation of phenol, 2-chlorophenol, and pentachlorophenol[4] and in the decomposition of salicylic acid.[5] The enhanced photocatalytic activity of coupled ZnO/TiO_2 can be interpreted on the basis of the process of electron transfer from the conduction band of ZnO to the conduction band of TiO_2 under illumination and by the hole transfer from the valence band of TiO_2 to the valence band of ZnO. This process gives rise to a decrease in the electron−hole pair recombination rate and an increase in lifespan. It also increases the availability of the pairs (electron and hole) on the surface of the photocatalyst and thus enhances the redox process.[6]

A wide variety of coupled polycrystalline structures that are synthesized through chemical approaches have core−shell (surface coating) or sandwich (particles adhere to each other) geometries.[7−12] Here, we report a simple method for the preparation of ZnO/TiO_2 nanohybrid structures by the site-specific deposition of titanium oxide on ZnO nanorods. Transmission electron microscopy (TEM) revealed each ZnO nanorod to be assembled with one TiO_2 cap at one end of the rod (the Zn-terminated (0001) surface). The polarity of the ZnO (0001) surface plays an important role in the formation of ZnO/TiO_2 nanohybrid structures. The phase transformation, stability, and interface structures of the nanohybrids were also systematically investigated.

Experimental Section

For the fabrication of ZnO/TiO_2 nanohybrid structures, 5 mL of 0.1 M zinc acetate ethanol solution was mixed with 35 mL of 0.5 M NaOH ethanol solution and 200 mg of amorphous titanium oxide powders (purity 99%, analytical reagent, China Guangdong Xilong Chemical Co., Ltd.) to form a suspension solution. The suspension solution was later transferred to a Teflon-lined stainless steel autoclave (50 mL) and heated at 180 °C for 24 h. White precipitation products that were obtained at the bottom of the autoclave were washed with ethanol and deionized water several times and then centrifuged and dried at 80 °C for further study. The yield of nanohybrids was about 50 mg per autoclave (50 mL). A drop of solution containing the product was diluted with ethanol and was sonicated for 15 min in ultrasonic cleaner (frequency: 40 kHz, Branson 3510) and then dispersed onto a perforated carbon film for structural characterization by using a JEOL JEM-2010F transmission electron microscope (operated at 200kV) that was equipped with an energy-dispersive X-ray spectrometer (EDX). Convergent-beam electron diffraction (CBED) patterns were recorded by using a Philips transmission electron microscope (CM120), and the CBED simulation was performed by using the JEMS simulation software. The as-prepared products were characterized by X-ray powder diffraction (XRD; Philips, PW1813). Differential scanning calorimetry (DSC) and thermogravimetry analysis (TGA) (NETZSCH STA 449C) measurements were carried out in a flowing Ar atmosphere at a constant heating rate of 10 °C/min. In addition, for comparison, the reactions in the absence of the amorphous titanium oxide (or zinc acetate) were also carried out with other conditions unchanged. A 35 mL portion of 0.5 M NaOH ethanol solution was mixed with 5 mL of 0.1 M zinc acetate ethanol solution (or 200 mg of the amorphous titanium oxide) to form a suspension solution. The suspension solution was later transferred into a Teflon-lined stainless steel autoclave (50 mL) and heated at 180 °C for 24 h. Without the amorphous titanium oxide, only ZnO

* Corresponding author. E-mail: phwang@ust.hk. Fax: 852-2351652. Tel: 852-23587489.

10.1021/jp0756911 CCC: $37.00 © xxxx American Chemical Society
Published on Web 10/13/2007 PAGE EST: 4.5

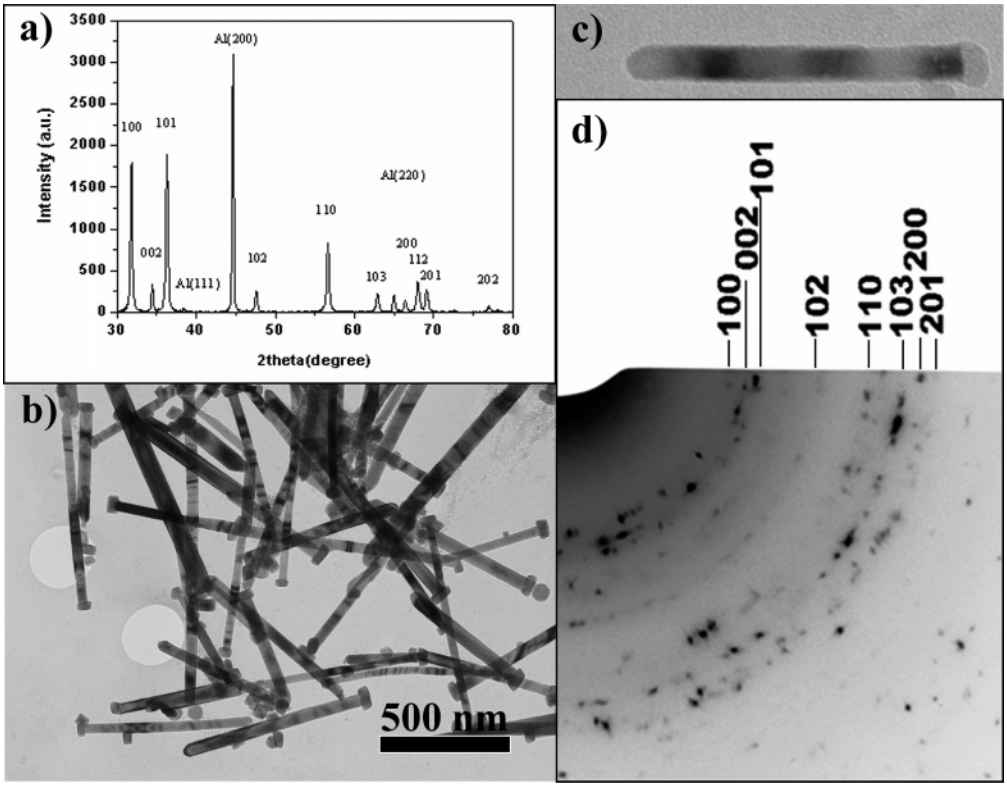

Figure 1. (a) XRD pattern of the as-prepared nanohybrid product. The reflections of ZnO crystal are marked by the indices. The Al peaks come from the aluminum holder in the XRD measurement. (b) TEM image showing the morphology of the fabricated ZnO/TiO_2 nanohybrid product. (c) TiO_2 nanoparticles assembled at one end of the ZnO nanorod only. (d) SAED pattern of the nanohybrid product.

nanowires (with diameters ranging from several nanometers to tens of nanometers and lengths of several micrometers) were obtained. Without zinc acetate, the product consists of amorphous TiO_2 nanoparticles only (tens of nanometers in size).

Results and Discussion

Figure 1a shows a representative XRD pattern of the as-prepared nanohybrid product. The diffraction peaks can be well indexed as a Wurtzite-type hexagonal-phase ZnO with the lattice parameters $a = 3.252$ Å and $c = 5.208$ Å, which is in good agreement with the calculated values $a = 3.253$ and $c = 5.209$ (JCPDS 80-0075). The typical morphology of the fabricated ZnO/TiO_2 nanohybrids is illustrated in Figure 1b. Each nanorod has one TiO_2 particle assembled at one end only (Figure 1c). Some TiO_2 particles were observed with the nanohybrids in the reaction solution because of the excessive titanium oxide source that was used. The selected-area electron diffraction (SAED) pattern (Figure 1d) of these nanohybrids shows that the ZnO nanorods are composed of Wurtzite-type hexagonal-phase (JCPDS 80-0075) crystals.

A high-resolution TEM (HRTEM) study showed the ZnO nanorods to be single crystalline and [0001] to be the preferential growth direction. This is illustrated in the HRTEM image in Figure 2a, which clearly shows the lattice spacing of 0.52 nm that corresponds to the interplane spacing of the (0001) planes of the Wurtzite-type hexagonal ZnO crystals. The ZnO nanorods were well crystallized, with no impurities being detected within the limit of the EDX. The titanium oxide particles that assembled to the nanorods were identified to be amorphous, and the stoichiometric ratio of Ti to O as measured by the EDX was about 1:2 (see Figure 2b). The interfaces between the ZnO nanorods and TiO_2 were flat and clearly visible when the electron beam was perpendicular to the nanorod axes. We believe that the TiO_2 nanoparticles might nucleate and grow on the end surfaces of the ZnO nanorods. Another possibility, however, is that TiO_2 particles in the solution might fuse preferentially with the nanorods tops and attached on the tips. Some cap-like TiO_2 particles can be seen in Figure 2c. Similar nanoparticles were observed in the experiment without adding zinc acetate.

Wurtzite-type ZnO has a polar crystalline structure that consists of Zn-terminated (0001) and O-terminated ($000\bar{1}$) surfaces. The CBED technique is conventionally used in TEM to determine the polarity of semiconductor compounds.[13−14] The CBED patterns are formed with a converged electron probe focusing on the sample area in the nanometer range. Figure 2d illustrates the CBED pattern along the [$1\bar{1}00$] zone axis. Because the diameters of most of the ZnO/TiO_2 nanorods were small, a thick ZnO/TiO_2 nanorod of about 80 nm in diameter was used with a low accelerating voltage (80 kV) of the electron beam for the CBED study to achieve a better contrast and to allow the determination of the number of Kossel−Moellenstedt fringes (or decrease in the extinction distance of the material) in the CBED pattern. In the CBED study, the thickness of the nanorod was estimated to be of the same order as the diameter. The fringes and intensities that are shown in diffraction disks (0002) and ($000\bar{2}$) in Figure 2d varied with the sample thickness. It can clearly be seen that the two disks are asymmetrical: the central diffraction fringe in the (0002) disk is a bright single line, whereas the central fringe in the ($000\bar{2}$) disk consists of bright double lines. This experimental CBED pattern matches fairly well with the simulated pattern (produced using JEMS simulation software) that is shown in Figure 2e. The best match was found for the sample thickness near 65 nm (with an electron beam energy of 80 kV). We investigated a number of ZnO/TiO_2 nanorods by using CBED and obtained the same result, namely, that the polar surfaces of the nanorods that were covered with TiO_2 caps had Zn-terminated (0001) surfaces.

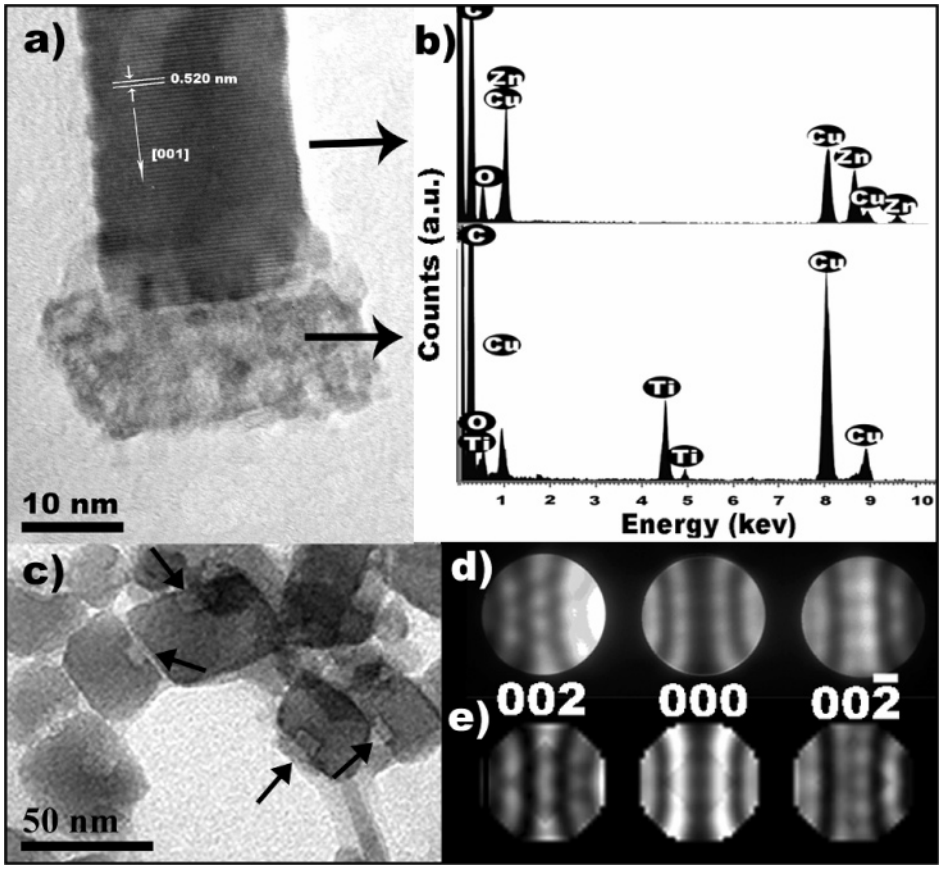

Figure 2. (a) HRTEM image of an individual ZnO/TiO_2 structure. (b) EDX spectra recorded by focusing the electron beam on the nanorod and the TiO_2 cap, respectively. The C and Cu signals come from a carbon-supporting film that was prepared on the copper grid. (c) The amorphous caps (the hole of each of which is indicated by the arrows) that may have become detached from the ZnO/TiO_2 nanohybrids during TEM sample preparation. (d) The CBED pattern taken along the [11$\bar{2}$0] direction. (e) The corresponding simulated CBED pattern.

To understand the mechanism of the formation of ZnO/TiO_2 nanohybrids, we investigated the initial growth process of ZnO nanorods and TiO_2 nanoparticles. ZnO nanorods of lengths of 100−200 nm were formed without any titanium oxide deposition at the tips or on the side surfaces within the first hour of reaction (see Figure 3a). During the second hour of reaction, a thin layer of amorphous titanium oxide gradually appeared on the (0001) planes and at the tips of the ZnO nanorods. After 3 h, the TiO_2 layers became obvious, as marked by the arrows in Figure 3b. As the reaction time increased, these thin layers of titanium oxide grew to cover the entire tips of the ZnO nanorods, developing a cap-like morphology (see Figure 1b). It was noted that the length of the nanorods increased very slowly after the formation of the amorphous titanium oxide on the nanorod tips. These experimental results confirm that the fastest nanorod growth occurs along the [0001] direction at a much faster rate than that along the (000$\bar{1}$) direction.[15] Because of the presence of the TiO_2, the growth of the ZnO nanorods along the [0001] direction was retarded by the "caps." Therefore, for the same reaction conditions, the ZnO nanorods that grew in the presence of TiO_2 were much shorter than the ZnO nanorods that grew without TiO_2.

On the basis of the observed growth conditions and structure, we believe that the formation of the ZnO/TiO_2 nanohybrids is due to the site-specific deposition of titanium oxide on the polar planes and tips of the ZnO nanorods. It is suggested that, for the ZnO with a Wurtzite structure, the Zn-terminated polar surface is chemically active in the growth of nanostructures.[16,17] The inherent asymmetry and anisotropy result in the preferential growth of the crystal along the *c*-axis, which is terminated by Zn ions.[14,15] The net dipole moment diverges as the length of the nanorod increases, and the electrostatic potential increases monotonically, which cannot be compensated by surface reconstruction because ZnO ± (0001) is quite stable.[18] To cancel out the polarity, a rearrangement of the charges on the outermost layers is proposed through the following three principal mech-

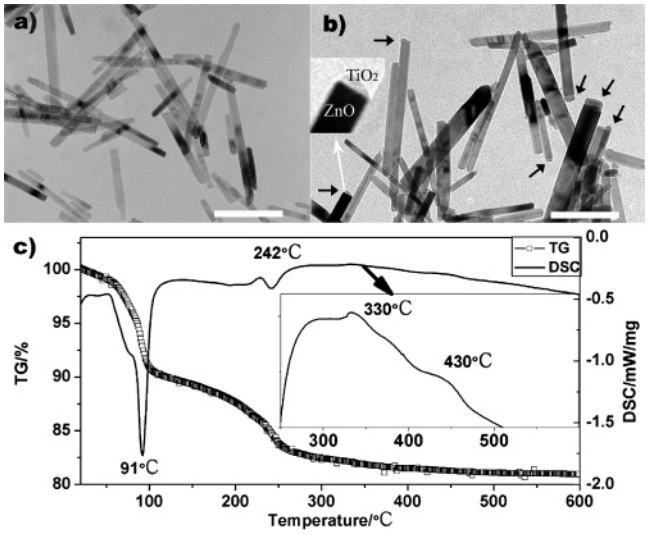

Figure 3. Typical TEM images of the products after (a) 1 h and (b) 3 h of reaction. The inset in panel b is an enlarged TEM image to show the big difference in the contrasts for a TiO_2 particle and a ZnO nanorod. Amorphous particles are marked with arrows. (c) DSC and TGA results for the nanohybrid product. The inset in panel c is the enlarged DSC curve for the temperature range of 250−500 °C. The scale bar is 100 nm.

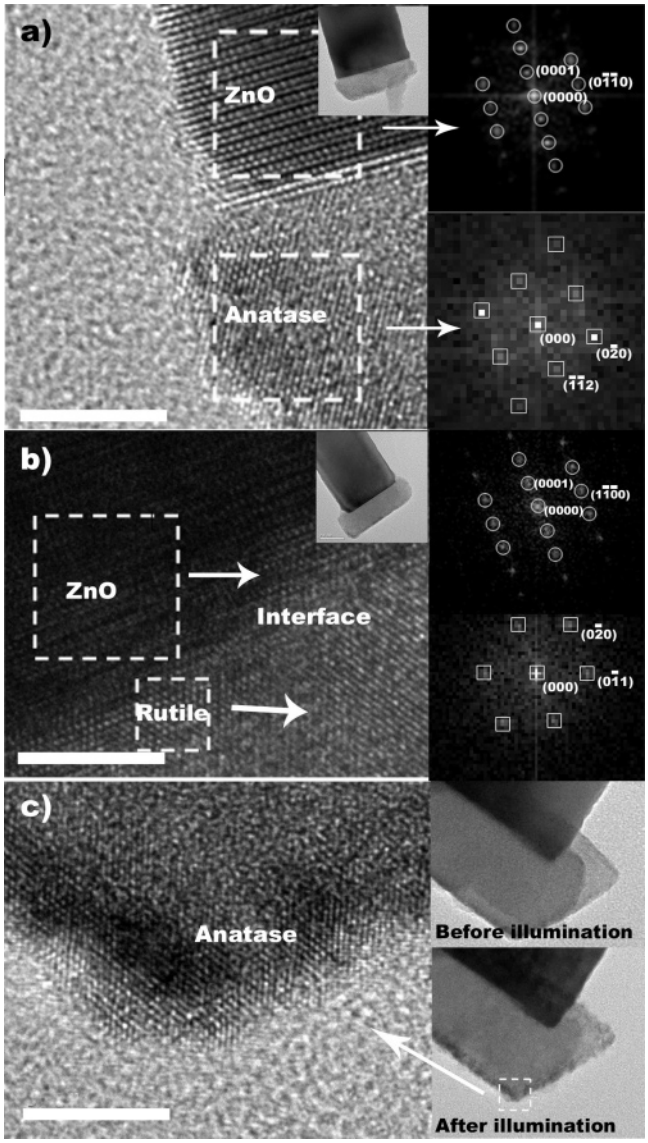

Figure 4. HRTEM images showing the phase transformation by annealing at (a) 300 °C and (b) 600 °C for 2 h. The insets show the low-magnification TEM images and the FFT patterns of the areas that are marked by the dashed lines in the main picture. The images were taken from the zone axes of $[11\bar{2}0]$ for ZnO, [201] for anatase TiO_2 (a), and [100] for rutile TiO_2 (b). (c) Anatase crystallites formed at the outermost shell of the cap after illumination with a convergent electron beam. The insets show images of the TiO_2 caps before and after electron beam illumination. The scale bar is 5 nm.

anisms: (1) the creation of surface states and the transfer of negative charges from the O-face to the Zn-face, (2) the removal of surface atoms, and (3) the deposition of positively (negatively) charged impurity atoms on the O (or Zn) surface.[19] In this experiment, the formation of the nanohybrids is believed to have been caused by the third compensation mechanism, with the outermost Zn-terminated (0001) faces of the nanorods adsorbing the anions and the outermost O-terminated $(000\bar{1})$ faces adsorbing the cations. Amorphous TiO_2 that was dissolved in alkali ethanol at a high temperature and under a high pressure generated a certain concentration of titanium hydrate colloids with negative charges.[20] These negative colloids were captured by the positive Zn-terminated (0001) faces of the nanorods, which resulted in the deposition of amorphous TiO_2 at the tips and the canceling out of the polarity of the nanorods. For the O-terminated $(000\bar{1})$ tips, however, we found that, after the formation of the TiO_2 caps at the (0001) tips, the $(000\bar{1})$ tips became tapered or rounded. In addition, we observed that the TiO_2 nanocaps could be assembled on ZnO nanorods of different diameters. ZnO/TiO_2 nanohybrids can also be achieved by using pre-synthesized ZnO nanorods as the starting materials and reacting them with TiO_2 alkali ethanol solution. By controlling the aspect ratios and diameters of the ZnO nanorod source material, it would be easy to fine-tune the aspect ratios and sizes of the TiO_2 caps on the nanohybrids.

The annealing of the nanohybrids at different temperatures revealed the occurrence of a phase transition in the titanium oxide caps. Figure 3c shows the DSC and TGA results for the nanohybrid product. The exothermic peaks with weight loss observed at ~91 and ~242 °C correspond to the removal of physically absorbed water and organic components. The small exothermic peaks that were observed at ~330 and ~430 °C without weight loss are associated with the phase transition of TiO_2 from an amorphous state to a crystalline state, such as an anatase or rutile structure. As observed in the low-magnification TEM images of the nanohybrids (see the insets in Figure 4a,b), there is no change in the morphologies of the ZnO nanorods and the titanium oxide caps after annealing the samples at 300 and 600 °C. Figure 4a,b illustrates the HRTEM images of titanium oxide caps that were annealed at 300 and 600 °C in air, respectively. Generally, the annealed titanium oxide caps consisted of several crystallites with almost the same orientation. In studying the HRTEM images and the corresponding fast Fourier transform (FFT), we identified that the amorphous titanium oxide was converted to the anatase phase at 300 °C and then to the rutile phase at 600 °C (see the insets in Figure 4a,b). The HRTEM image in Figure 4 was taken with the electron beam parallel to the zone axes of $[11\bar{2}0]$ for ZnO, [201] for the anatase TiO_2, and [100] for the rutile TiO_2. We observed that the temperature that was needed for the crystallization of the amorphous titanium oxide to occur was quite low. This may be attributable to the size effect of the nanoparticles (a low melting temperature compared to that of the bulk material) or to organic impurities that remained on the surface of the titanium oxide caps.[21] When the amorphous titanium oxide cap was illuminated by a strong convergent electron beam, the apparent crystallization of the amorphous titanium oxide to the anatase structure occurred at the outermost shell of the cap. This is shown in Figure 4c, in which the area of crystallization is shaded dark to contrast it with the inner part. The FFT analysis revealed the TiO_2 crystallites of the anatase and rutile phases to have the following orientation relationships with the ZnO nanorods:

$$(112)_{TiO_2\ anatase} \,||\, (0001)_{ZnO}$$

$$[201]_{TiO_2\ anatase} \,||\, [11\bar{2}0]_{ZnO}$$

$$(011)_{TiO_2\ rutile} \,||\, (0001)_{ZnO}$$

$$[100]_{TiO_2\ rutile} \,||\, [11\bar{2}0]_{ZnO}$$

The interplane spacing $d_{(112)/TiO_2\ anatase}$ (2.33 Å) was close to $d_{(011)/TiO_2\ rutile}$ (2.46 Å), and both planes were parallel to the $(0001)_{ZnO}$ after the phase transition. We found the crystallites that were formed by annealing or electron beam irradiation to have a very similar orientation relationship with the ZnO nanorods. The interface structures of almost all of the nanohybrids were similar and atomically flat. It is expected that such uniform interfaces will generate good electrical contact between the ZnO and TiO_2 nanocrystals, which may enhance the interfacial charge-transfer processes of the photogenerated

charge carriers and thus the photocatalytic activity of the nanocomposite material. Because different crystal phases of TiO_2 show distinct chemical properties, the present synthesis method also provides an effective way to fabricate and control ZnO/TiO_2 nanocomposite structures for use in a host of technological applications.

Conclusion

In summary, we have demonstrated a simple method of synthesizing ZnO/TiO_2 nanohybrid structures by the site-specific deposition of titanium oxide on ZnO nanorods. The polarity of the ZnO (0001) surface plays an important role in the formation of ZnO/TiO_2 nanohybrid structures. Annealing at different temperatures gives rise to the phase transformation of amorphous TiO_2 to anatase phase and rutile phase nanocrystals with good interface structures. This work provides a rational approach to the assembly of complex nanohybrids using the intrinsic properties of ZnO nanocrystals that allows the size, aspect ratio, and TiO_2 cap structures to be fully controlled in the fabrication process and by subsequent annealing treatments.

Acknowledgment. The authors are grateful for the technical assistance of K. M. Ho of the Department of Physics at HKUST. This work was financially supported by the Research Grants Council of Hong Kong (Project Nos. N_HKUST615/06 and CityU 3/04C).

References and Notes

(1) Pacholski, C.; Kornowski, A.; Weller, H. *Angew. Chem., Int. Ed.* **2004**, *43*, 4774.

(2) Cozzoli, P. D.; Curri, M. L.; Giannini, C.; Agostiano, A. *Small* **2006**, *2*, 413.

(3) Jakob, M.; Levanon, H.; Kamat, P. V. *Nano Lett.* **2003**, *3*, 353.

(4) Serpone, N.; Maruthamuthu, P.; Pichat, P.; Pelizzetti, E.; Hidaka, H. J. *Photochem. Photobiol. A: Chem.* **1995**, *85*, 247.

(5) Sukharev, V.; Kershaw, R. *Photochem. Photobiol. A: Chem.* **1996**, *98*, 165.

(6) Marci, G.; Augugliaro, V.; Lopez-Munoz, M. J.; Martin, C.; Palmisano, L.; Rives, V.; Schiavello, M.; Tilley, R. J. D.; Venezia, A. M. *J. Phys. Chem. B* **2001**, *105*, 1033.

(7) Chueh, Y. L.; Chou, L. J.; Wang, Z. L. *Angew. Chem., Int. Ed.* **2006**, *45*, 7773.

(8) Shi, W.; Zeng, H.; Sahoo, Y.; Ohulchanskyy, T. Y.; Ding, Y.; Wang, Z. L.; Swihart, M.; Prasad, P. N. *Nano Lett.* **2006**, *6*, 875.

(9) Kwon, K.-W.; Shim, M. *J. Am. Chem. Soc.* **2005**, *127*, 10269.

(10) Casavola, M.; Grillo, V.; Carlino, E.; Giannini, C.; Gozzo, F.; Pinel, E. F.; Garcia, M. A.; Manna, L.; Cingolani, R.; Cozzoli, P. D. *Nano Lett.* **2007**, *7*, 1386.

(11) Buonsanti, R.; Grillo, V.; Carlino, E.; Giannini, C.; Curri, M. L.; Innocenti, C.; Sangregorio, C.; Achterhold, K.; Parak, F. G.; Agostiano, A.; Cozzoli, P. D. *J. Am. Chem. Soc.* **2006**, *128*, 16953.

(12) Yu, H.; Chen, M.; Rice, P. M.; Wang, S. X.; White, R. L.; Sun, S. H. *Nano Lett.* **2005**, *5*, 379.

(13) Ponce, F. A.; Bour, D. P.; Young, W. T.; Saunders, M.; Steeds, J. W. *Appl. Phys. Lett.* **1996**, *69*, 337.

(14) Zou, K.; Qi, X. Y.; Duan, X. F.; Zhou, S. M.; Zhang, X. H.; *Appl. Phys. Lett.* **2005**, *86*, 013103.

(15) Li, W. J.; Shi, E. W.; Zhong, W. Z.; Yin, Z. W. *J. Cryst. Growth* **1999**, *203*, 186.

(16) Wang, Z. L.; Kong, X. Y.; Zuo, J. M. *Phy. Rev. Lett.* **2003**, *91*, 185502.

(17) Wang, Z. L. *J. Mater. Chem.* **2005**, *15*, 1021.

(18) Meyer, B.; Marx, D. *Phys. Rev. B* **2003**, *67*, 035403.

(19) Dulub, O.; Diebold, U.; Kresse, G. *Phy. Rev. Lett.* **2003**, *90*, 016102.

(20) Yang, H. G.; Li, C. Z.; Gu, H. C.; Fang, T. N.; *J. Colloid Interface Sci.* **2001**, *236*, 96

(21) John, A. K.; Surender, G. D. *J. Mater. Sci.* **2005**, *40*, 2999.